A Study on Using Hierarchical Basis Error Estimates in Anisotropic Mesh Adaptation for the Finite Element Method

Lennard Kamenski

Department of Mathematics, The University of Kansas, lkamenski@math.ku.edu

Summary. A common approach for generating an anisotropic mesh is the *M-uniform mesh* approach where an adaptive mesh is generated as a uniform one in the metric specified by a given tensor M. A key component is the determination of an appropriate metric which is often based on some type of Hessian recovery. This study discusses the use of a hierarchical basis error estimator for the development of an anisotropic metric tensor needed for the adaptive finite element solution. A global hierarchical basis error estimator is employed to obtain reliable directional information. Numerical results for a selection of different applications show that the method performs comparable with existing metric tensors based on Hessian recovery and can provide even better adaptation to the solution if applied to problems with gradient jumps and steep boundary layers.

Key words: mesh adaptation, anisotropic mesh, finite element, a posteriori estimate, hierarchical basis, variational problem, anisotropic diffusion

1 Introduction

A common approach for generating an anisotropic mesh is the *M-uniform mesh* approach based on generation of a quasi-uniform mesh in the metric space defined by a symmetric and strictly positive definite metric tensor M. A scalar metric tensor will lead to an isotropic mesh while a full metric tensor will generally result in an anisotropic mesh. In this sense, the mesh generation procedure is the same for both isotropic and anisotropic mesh generation. A key component of the approach is the determination of an appropriate metric often based on some type of error estimates.

Typically, the appropriate metric tensor depends on the Hessian of the exact solution of the underlying problem, which is often unavailable in practical computation, thus requiring the recovery of an approximate Hessian from the computed solution. A number of recovery techniques are used for this purpose, for example the gradient recovery technique by Zienkiewicz and Zhu [34, 35], the technique based on the variational formulation by Dolejší [17], or

the quadratic least squares fitting (QLS) proposed by Zhang and Naga [33]. Generally speaking, Hessian recovery methods work well when exact nodal function values are provided (e.g. interpolation problems), but unfortunately they do not provide an accurate recovery when applied to linear finite element approximations on non-uniform meshes, as pointed out by the author in [28]. Recently, conditions for asymptotically exact gradient and convergent Hessian recovery from a hierarchical basis error estimator have been given by Ovall [31]. His result is based on superconvergence results by Bank and Xu [7, 8], which require the mesh to be uniform or almost uniform: assumptions which are usually violated by adaptive meshes.

Hence, a convergence of adaptive algorithms based explicitly on the Hessian recovery cannot be proved in a direct way, even if their application is quite successful in practical computations [17, 26, 29]. This explains the recent interest in anisotropic adaptation strategies based on some type of *a posteriori* error estimates. For example, Cao et al. [12] studied two a posteriori error estimation strategies for computing scalar monitor functions for use in adaptive mesh movement; Apel et al. [5] investigated a number of *a posteriori* strategies for computing error gradients used for directional refinement; and Agouzal et al. [1, 2, 3] and Agouzal and Vassilevski [4] proposed a new method for computing metric tensors to minimize the interpolation error provided that an edge-based error estimate is given.

Recently, Huang et al. [24] presented a mesh adaptation method based on hierarchical basis error estimates (HBEE). The new framework is developed for the linear finite element solution of a boundary value problem of a second-order elliptic partial differential equation (PDE), but it is quite general and can easily be adopted to other problems. A key idea in the new approach is the use of the globally defined HBEE for the reliable directional information: globally defined error estimators have the advantage that they contain more directional information of the solution; error estimation based on solving local error problems, despite its success in isotropic mesh adaptation, do not contain enough directional information, which is global in nature; moreover, Dobrowolski et al. [16] have pointed out that local error estimates can be inaccurate on anisotropic meshes.

The objective of this article is to study the application of this new anisotropic adaptation method to different problems. A brief description of the method is provided in Sect. 2. An example of its application to a boundary value problem of a second-order elliptic PDE is given in Sect. 3 for heat conduction in a thermal battery with large and orthotropic jumps in the material coefficients.[1] Section 4 presents an anisotropic metric tensor for general variational problems developed by Huang et al. [25] using the HBEE and the underlying variational formulation and gives a numerical example for a non-quadratic variational problem. The metric tensor is completely *a posteriori*: it is based solely on the residual, edge jumps, and the *a posteriori* error

[1] A Sandia National Laboratories benchmark problem.

estimate. The third example is an anisotropic diffusion problem. The exact solution of this problem satisfies the maximum principle and it is desirable for the numerical solution to fulfill its discrete counterpart: the discrete maximum principle (DMP). Recently, Li and Huang [29] developed an anisotropic metric tensor based on the anisotropic non-obtuse angle condition, which provides both mesh adaptation and DMP satisfaction for the numerical solution: the mesh alignment is determined by the main diffusion drag direction, i.e. by the underlying PDE, and the Hessian of the exact solution determines the optimal mesh density. In Sect. 5, the Hessian of the exact solution is replaced with the Hessian of the hierarchical error estimator to obtain a new, completely *a posteriori*, metric tensor accounting for both DMP satisfaction and mesh adaptation. Concluding remarks on the numerical examples and some key components of the hierarchical basis error estimator are given in Sect. 6.

2 Anisotropic mesh adaptation based on hierarchical basis error estimator

Consider the solution of a variational problem: find $u \in V$ such that

$$a(u, v) = f(v) \quad \forall v \in V \tag{P}$$

where V is an appropriate Hilbert space of functions over a domain $\Omega \in \mathbb{R}^2$, $a(\cdot, \cdot)$ is a bilinear form defined on $V \times V$, and $F(\cdot)$ is a continuous linear functional on V. The linear finite element approximation u_h of u is the solution of the corresponding variational problem in a finite dimensional subspace $V_h \subset V$ of piecewise linear functions: find $u_h \in V_h$ such that

$$a(u_h, v_h) = f(v_h) \quad \forall v_h \in V_h. \tag{P_h}$$

For the adaptive finite element solution, the mesh $\mathcal{T}_h$ is generated according to the behaviour of the error of the approximation u_h. This study follows the M-uniform mesh approach [23] which generates an adaptive mesh as a uniform mesh in the metric specified by a symmetric and strictly positive definite tensor $M = M(\boldsymbol{x})$. Such a mesh is called an *M-uniform mesh*. Once a metric tensor M has been chosen, a sequence of mesh and corresponding finite element approximation are generated in an iterative fashion.

An adaptive algorithm starts with an initial mesh $\mathcal{T}_h^{(0)}$. On every mesh $\mathcal{T}_h^{(i)}$ the variational problem (P_h) with $V_h^{(i)}$ is solved and the obtained approximation $u_h^{(i)}$ is used to compute a new adaptive mesh for the next iteration step. The new mesh $\mathcal{T}_h^{(i+1)}$ is generated as a M-uniform mesh with a metric tensor $M_h^{(i)}$ defined in terms of $u_h^{(i)}$. This yields the sequence

$$(\mathcal{T}_h^{(0)}, V_h^{(0)}) \to u_h^{(0)} \to M_h^{(0)} \to (\mathcal{T}_h^{(1)}, V_h^{(1)}) \to u_h^{(1)} \to M_h^{(1)} \to \dots$$

The process is repeated until a good adaptation is achieved. In the computation, the mesh generation software *bamg* (*bidimensional anisotropic mesh generator* developed by F. Hecht [21]) is used to generate new adaptive meshes. The mesh adaptation quality is characterized by the alignment and equidistribution quality measures introduced in [22]; more details can be found in [24, Sect. 4.1].

2.1 Adaptation based on *a posteriori* error estimates

Typically, the metric tensor M_h depends on the Hessian of the exact solution of the underlying problem [19, 23]. As mentioned in Sect. 1, it is not possible to obtain an accurate Hessian recovery from a linear finite element solution in general [28], so there is no way to prove a convergence of an adaptive algorithm based on the Hessian recovery in a direct way, even if its application is quite successful in practical computations [17, 26, 29].

An alternative approach developed in [24] employs an *a posteriori* error estimator for defining and computing M_h. The brief idea is as follows.

Assume that an error estimate z_h is reliable in the sense that

$$\|u - u_h\| \leq C \|z_h\| . \tag{1}$$

for a given norm $\|\cdot\|$ and that it has the property

$$\Pi_h z_h \equiv 0 \tag{2}$$

for some interpolation operator Π_h. Then the finite element approximation error is bounded by the (explicitly computable) interpolation error of the error estimate z_h, viz.,

$$\|u - u_h\| \leq C \|z_h\| = C \|z_h - \Pi_h z_h\| . \tag{3}$$

Now, it is known from the interpolation theory [27] that the interpolation error for a given function v can be bounded by a term depending on the triangulation $\mathcal{T}_h$ and derivatives of v, i.e.,

$$\|v - \Pi_h v\| \leq C \, \mathcal{E}(\mathcal{T}_h, v),$$

where C is a constant independent of $\mathcal{T}_h$ and v. Therefore, we can rewrite (3) as

$$\|u - u_h\| \leq C \, \mathcal{E}(\mathcal{T}_h, z_h).$$

In other words, up to a constant, the solution error is bounded by the interpolation error of the error estimate. Thus, the metric tensor M_h can be constructed to minimize the interpolation error of the z_h and does not depend on the Hessian of the exact solution.

2.2 Hierarchical basis *a posteriori* error estimate

One possibility to achieve the property (2) is to use the hierarchical basis error estimator. The general framework can be found among others in the work of Bank and Smith [6] or Deuflhard et al. [15]. The approach is briefly explained as follows.

Let $e_h = u - u_h$ be the error of the linear finite element solution $u_h \in V_h$. Then for all $v \in V$ we have

$$a(e_h, v) = f(v) - a(u_h, v). \tag{E}$$

Let $\bar{V}_h = V_h \oplus W_h$ be a space of piecewise quadratic functions, where W_h is the linear span of the quadratic edge bubble functions (a quadratic edge bubble function is defined as a product of the two linear nodal basis functions corresponding to the edge endpoints). If $\mathit{\Pi}_h$ is defined as the vertex-based, piecewise linear Lagrange interpolation then it satisfies (2) since the edge bubble functions vanish at vertices.

The error estimate z_h is then defined as the solution of the approximate error problem: find $z_h \in W_h$ such that

$$a(z_h, w_h) = f(w_h) - a(u_h, w_h) \quad \forall w_h \in W_h. \tag{E_h}$$

The estimate z_h can be viewed as a projection of the true error onto the subspace W_h. Then, if assumption (1) holds, the finite element approximation error can be controlled by minimizing the interpolation error of z_h, i.e., the right-hand side in (3).

Note that this definition of the error estimate is global and its solution can be costly. To avoid the expensive exact solution in numerical computation, only a few sweeps of the symmetric Gauss-Seidel iteration are employed for the resulting linear system, which proves to be sufficient for the purpose of mesh adaptation (see [24] for more details).

3 Boundary value problem of a second-order elliptic PDE

Consider two-dimensional heat conduction in a thermal battery with large orthotropic jumps in the material coefficients. This is an example provided in [24]; the mathematical model considered here is taken from [30, 32] and described by

$$\begin{cases} \nabla \cdot (\mathbb{D}^k \nabla u) = f^k & \text{in } \mathit{\Omega}, \\ \mathbb{D}^k \nabla u \cdot n = g^i - \alpha^i u & \text{on } \partial\mathit{\Omega}, \end{cases} \tag{4}$$

with $\mathit{\Omega} = (0, 8.4) \times (0, 24)$ and

$$\mathbb{D}^k = \begin{bmatrix} D_x^k & 0 \\ 0 & D_y^k \end{bmatrix}.$$

Region k	D_x^k	D_y^k	f^k
1	25	25	0
2	7	0.8	1
3	5	0.0001	1
4	0.2	0.2	0
5	0.05	0.05	0

Boundary i	α^i	g^i
1	0	0
2	1	3
3	2	2
4	3	0

Table 1: Heat conduction in a thermal battery: material coefficients D^k and boundary conditions (clockwise starting with the left-hand side boundary).

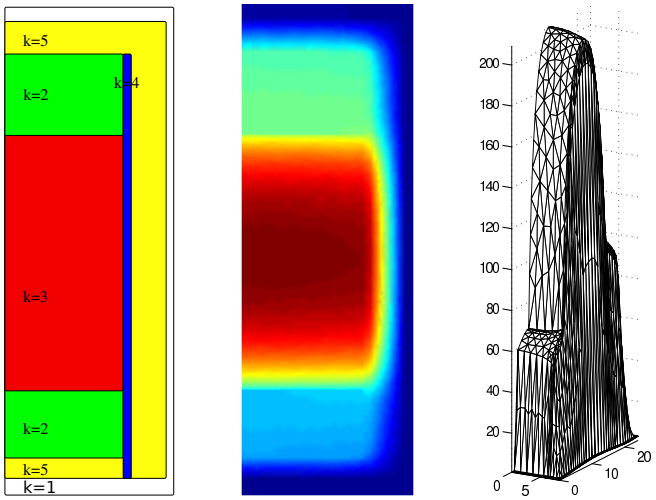

(a) (b) (c)

Fig. 1: Heat conduction in a thermal battery: (a) device geometry, (b) contour and (c) surface plots of a linear finite element solution.

Material coefficients D^k and the boundary conditions starting with the left-hand side boundary and ordering them clockwise are provided in Table 1. The analytical solution for this problem is unavailable, but the geometry and the contour and surface plots of a numerical approximation obtained with adaptive linear finite elements are given in Fig. 1.

For this problem, we follow the approach described in the previous section and employ the metric tensor developed in [24] for a boundary value problem of a second-order elliptic PDE. In two dimensions and for the error measured in the L^2-norm, the metric tensor $M_{HB,K}$ based on the HB error estimator is given element-wise by

$$M_{HB,K} = \det\left(I + \frac{1}{\alpha_h}\left|H_K(z_h)\right|\right)^{-\frac{1}{6}}\left[I + \frac{1}{\alpha_h}\left|H_K(z_h)\right|\right], \tag{5}$$

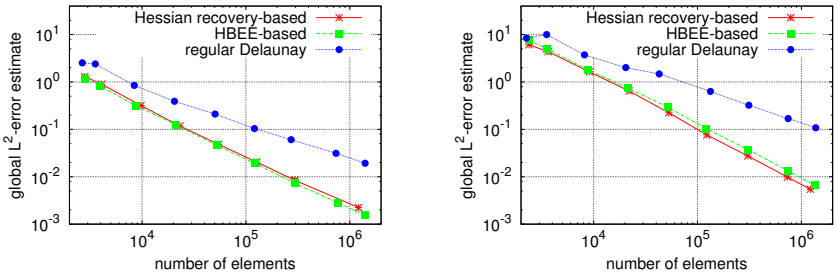

(a) With interface edges. (b) Without interface edges.

Fig. 2: Heat conduction in a thermal battery: a comparison of the error estimate for adaptive finite element solutions.

where $H_K(z_h)$ is the Hessian of the quadratic hierarchical basis error estimate z_h on element K and α_h is a regularization parameter to ensure that M_{HB} is strictly positive definite (see [24] for more details on the choice of α_h).

Figure 2 shows global error estimates (obtained by solving exactly the approximate error problem (E_h)) for finite element solutions on adaptive meshes controlled by the HBEE or quadratic least squares Hessian recovery (QLS) and having all or no predefined interface edges. Both methods provide comparable results.

Typical adaptive meshes with predefined interface edges for the HBEE and the QLS are shown in Fig. 3. When the mesh contains all the information of the interface, the QLS-based method produces a mesh with strong element concentration near all internal interfaces (Fig. 3a), whereas the HBEE leads to a mesh (cf. Fig. 3b) that has higher element concentration in the corners of the regions, has a proper element orientation near the interfaces between the regions 2 and 3, and is almost uniform in regions where the solution is nearly linear (cf. Fig. 1c for the surface plot of a computed solution). The maximum aspect ratio[2] of the mesh obtained by means of the HBEE is slightly larger.

When the interface edges are not present in the mesh, both methods provide similar results: the interfaces are recognized by both methods and the obtained adaptive meshes are dense near the interfaces, in order to resolve the gradient jumps.

This example result shows that Hessian recovery can lead to over-adaptation for non-smooth solutions. HBEE-based method, on the other hand, produces only necessary concentration and is also able to catch the directional information of the solution required for proper mesh alignment. This example particularly demonstrates that the HBEE-based method can be advantageous if applied to problems with jumping coefficients and strong anisotropic features.

[2]In this paper, aspect ratio is defined as the longest edge divided by the shortest altitude. An equilateral triangle has an aspect ratio of $\sqrt{3}/2 \approx 0.87$.

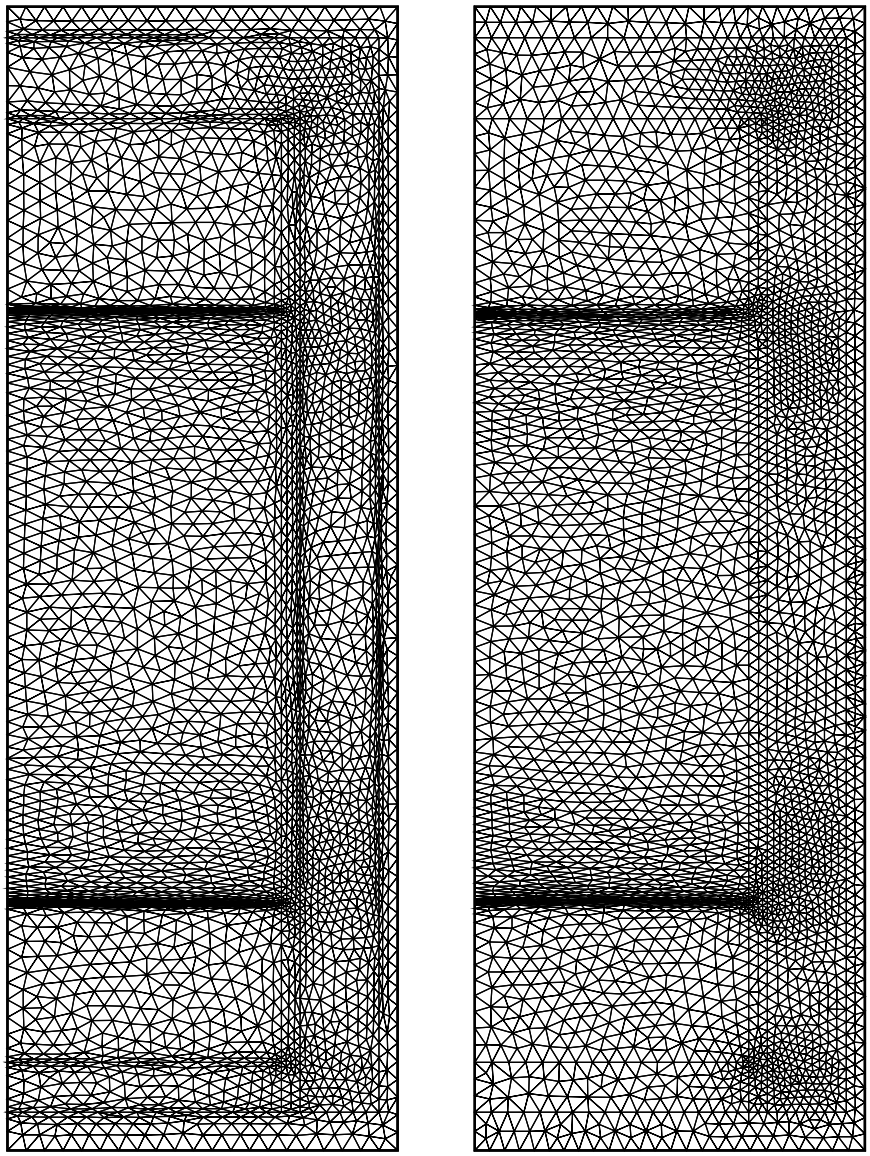

(a) QLS Hessian recovery: 6781 triangles, max. aspect ratio 39.2.

(b) HBEE: 6750 triangles, max. aspect ratio 54.8.

Fig. 3: Heat conduction in a thermal battery: adaptive meshes obtained with (a) quadratic least squares Hessian recovery and (b) the HBEE.

4 Variational problems

While it has attracted considerable attention from many researchers and been successfully applied to the numerical solution of PDEs, anisotropic mesh adaptation has rarely been employed for variational problems, especially when combined with *a posteriori* error estimates. Often, a variational problem can be transformed into a boundary value problem of partial differential equations (PDEs) and solved by methods designed for PDEs. Unfortunately, these methods do not take structural advantage of variational problems and many researchers argue that the variational formulation should be used as a natural optimality criterion for mesh adaptation. Recently, Huang and Li [26] developed a metric tensor for the adaptive finite element solution of variational problems. In the anisotropic case, it is semi-*a posteriori*: it involves residual and edge jumps, both dependent on the computed solution, and the Hessian of the exact solution. In [25], this result was improved to provide a metric tensor for variational problems based on the HBEE and the underlying variational formulation. The new metric tensor is *a posteriori* in the sense that it is based solely on residual, edge jumps, and HBEE. This is in contrast to most previous work where M depends on the Hessian of the exact solution and is semi-*a posteriori* or completely *a priori*; e.g., see [10, 11, 13, 20, 23, 26].

4.1 General variational problem and the anisotropic metric tensor

Consider a general functional of the form

$$I[v] = \int_\Omega F(\boldsymbol{x}, v, \nabla v) d\boldsymbol{x}, \quad \forall v \in V_g$$

where $F(\cdot,\cdot,\cdot)$ is a given smooth function, $\Omega \subset \mathbb{R}^d$ $(d = 1, 2, 3)$ is the physical domain and V_g is a properly selected set of functions satisfying the Dirichlet boundary condition

$$v(\boldsymbol{x}) = g(\boldsymbol{x}) \quad \forall \boldsymbol{x} \in \partial\Omega$$

for a given function g.

The corresponding variational problem is to find a minimizer $u \in V_g$ such that

$$I[u] = \min_{v \in V_g} I[v].$$

A necessary condition for u to be a minimizer is that the first variation of the functional vanishes. This leads to the Galerkin formulation

$$\delta I[u, v] \equiv \int_\Omega \left(F_u(\boldsymbol{x}, u, \nabla u)\, v + F_{\nabla u}(\boldsymbol{x}, u, \nabla u) \cdot \nabla v\right) d\boldsymbol{x} = 0 \tag{6}$$

for all $v \in V_0$, where $V_0 = V_g$ with $g = 0$ and F_u and $F_{\nabla u}$ are the partial derivatives of F with respect to u and ∇u, respectively.

Given a triangulation $\mathcal{T}_h$ for Ω and the associated linear finite element space $V_g^h \subset V_g$, the finite element solution u_h can be found by solving the corresponding Galerkin formulation: find $u_h \in V_g^h$ such that

$$\delta I[u_h, v_h] = \int_\Omega \left(F_u(\boldsymbol{x}, u_h, \nabla u_h)\, v_h + F_{\nabla u}(\boldsymbol{x}, u_h, \nabla u_h) \cdot \nabla v_h\right) d\boldsymbol{x} = 0$$

for all $v_h \in V_0^h$.

The *a posteriori* metric tensor $M_{VP,K}$ for general variational problems developed in [25] for the error measured in the H^1-semi-norm is given element-wise by

$$M_{VP,K} = \left(1 + \frac{1}{\alpha_h |K|}\left(|K|^{1/2} \|r_h\|_{L^2(K)} + \sum_{\gamma \in \partial K} |\gamma|^{1/2} \|R_h\|_{L^2(\gamma)}\right)\right)^{\frac{1}{2}} \times \det\left(I + \frac{1}{\alpha_h}|H_K(z_h)|\right)^{-\frac{1}{4}} \left[I + \frac{1}{\alpha_h}|H_K(z_h)|\right] \tag{7}$$

with the residual

$$r_h(\boldsymbol{x}) = F_u(\boldsymbol{x}) - \nabla \cdot F_{\nabla u}(\boldsymbol{x}) \qquad \boldsymbol{x} \in K \quad \forall K \in \mathcal{T}_h$$

and the edge jump

$$R_h(\boldsymbol{x}) = \begin{cases} (F_{\nabla u}(\boldsymbol{x}) \cdot \boldsymbol{n}_\gamma)|_K + (F_{\nabla u}(\boldsymbol{x}) \cdot \boldsymbol{n}_\gamma)|_{K'} & \boldsymbol{x} \in \gamma \quad \forall \gamma \in \partial\mathcal{T}_h \backslash \partial\Omega, \\ 0 & \boldsymbol{x} \in \gamma \quad \forall \gamma \in \partial\Omega. \end{cases}$$

Note, that $\delta I[u, v]$ in (6) is linear in v but is nonlinear in u in general. Thus, a modification of the error problem (E_h) for z_h in Sect. 2.2 is required. For this purpose, denote by $a_h(u_h; \cdot, \cdot)$ a bilinear form resulting from a linearization of $\delta I[\cdot, \cdot]$ about u_h with respect to the first argument. The error estimate z_h is then defined as the solution of the approximate *linear* error problem: find $z_h \in W^h$ such that

$$a_h(u_h; z_h, w_h) = -\delta I[u_h, w_h]$$

for all $w_h \in W^h$ [6].

4.2 Numerical example

Consider an anisotropic variational problem defined by the non-quadratic functional

$$I[u] = \int_\Omega \left[\left(1 + |\nabla u|^2\right)^{3/4} + 1000 u_y^2\right] d\boldsymbol{x}$$

with $\Omega = (0, 1) \times (0, 1)$ and the boundary condition

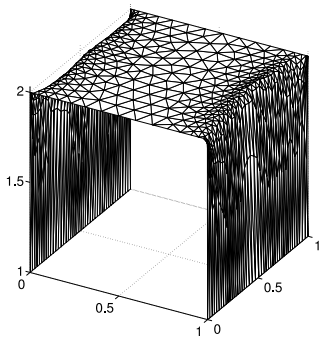

Fig. 4: Variational problem: surface plot of the numerical solution.

$$\begin{cases} u = 1 & \text{on } x = 0 \text{ or } x = 1, \\ u = 2 & \text{on } y = 0 \text{ or } y = 1. \end{cases}$$

This example is discussed in [25, 26] and is originally taken from [9]; the analytical solution is not available, but a computed solution in Fig. 4 shows that the mesh adaptation challenge for this example is the resolution of the sharp boundary layers near $x = 0$ and $x = 1$.

Adaptive meshes obtained with both metric tensors (Hessian recovery-based and HBEE-based) are given in Fig. 5. The both methods have correct mesh concentration and provide good alignment with the boundary layers. Anisotropic meshes are comparable, although mesh elements near the boundary layer in the HBEE-based adaptive mesh have a larger aspect ratio than elements of the mesh obtained by means of the Hessian recovery. This could be due to the smoothing nature of the Hessian recovery: usually, it operates on a larger patch, thus introducing an additional smoothing effect, which affects the grading of the elements' size and orientation. The global hierarchical basis error estimator does not have this handicap and, in this example, the mesh obtained by means of HBEE is slightly better aligned with the steep boundary layers.

5 Anisotropic diffusion problems and the DMP

Anisotropic diffusion problems arise in various areas of science and engineering, for example image processing, plasma physics, or petroleum engineering. Standard numerical methods can produce spurious oscillations when they are used to solve these problems. A common approach to avoid this difficulty is to design a proper numerical scheme or a mesh so that the numerical solution satisfies the discrete counterpart (DMP) of the maximum principle satisfied by the continuous solution. A well known condition for the DMP satisfaction by the linear finite element solution of isotropic diffusion problems is the

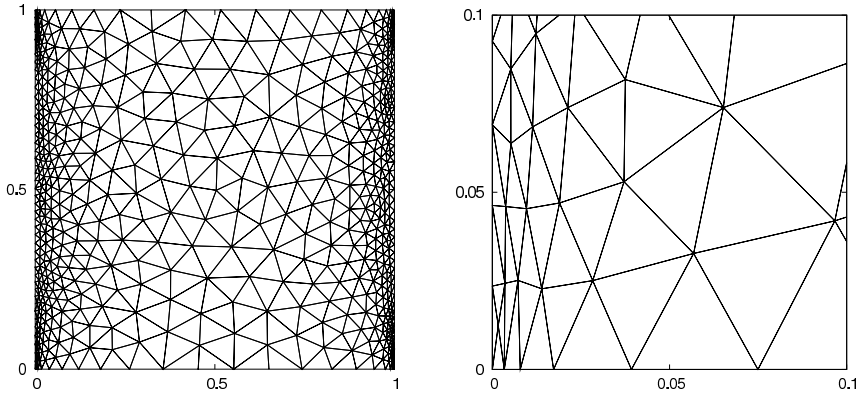

(a) Metric based on residual, edge jumps, and Hessian recovery: 1160 triangles, max. aspect ratio 15.

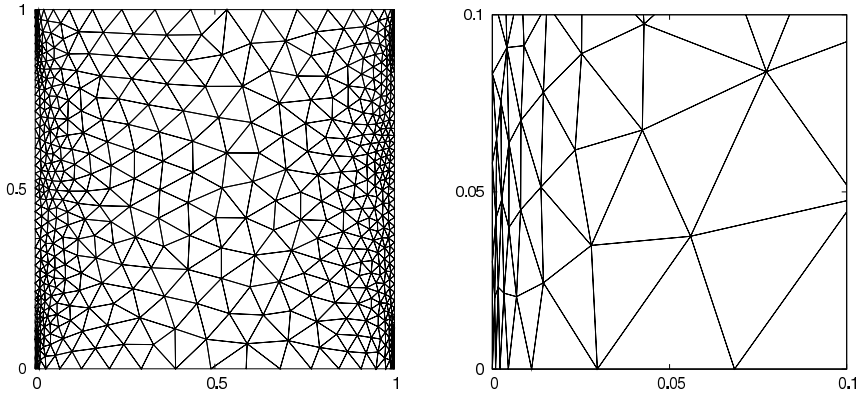

(b) Metric based on residual, edge jumps, and HBEE: 1143 triangles, max. aspect ratio 51.

Fig. 5: Variational problem: adaptive meshes obtained by means of Hessian recovery-based and HBEE-based metric tensors; close-up views at (0,0).

non-obtuse angle condition that requires the dihedral angles of mesh elements to be non-obtuse [14]. In [29], a generalization of the condition, the so-called anisotropic non-obtuse angle condition, was introduced for the finite element solution of heterogeneous anisotropic diffusion problems. The new condition is essentially the same as the existing one except that the dihedral angles are measured in a metric depending on the diffusion matrix of the underlying problem. Based on the new condition, a metric tensor for anisotropic mesh adaptation was developed, which combines the satisfaction of the DMP with mesh adaptivity. The obtained metric tensor is based on the diffusion matrix and the Hessian of the exact solution. As in previous sections, we can improve

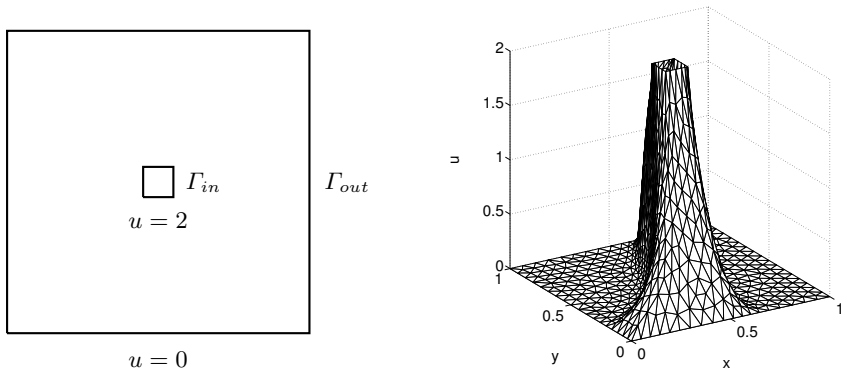

(a) Boundary conditions. (b) Numerical solution.

Fig. 6: Anisotropic diffusion: boundary conditions and numerical solution.

the obtained metric tensor by replacing the (unknown) Hessian of the exact solution by the Hessian of the HBEE as shown in the following example.

Consider the BVP discussed in [29]:

$$\begin{cases} \nabla \cdot (\mathbb{D}\,\nabla u) = f & \text{in } \Omega, \\ u = g & \text{on } \partial\Omega, \end{cases} \tag{8}$$

with

$$f \equiv 0, \quad \Omega = [0,1]^2 \backslash \left[\frac{4}{9}, \frac{5}{9}\right]^2, \quad g = 0 \text{ on } \Gamma_{out}, \quad g = 2 \text{ on } \Gamma_{in},$$

where Γ_{out} and Γ_{in} are the outer and inner boundaries of Ω, respectively (Fig. 6a). The diffusion matrix is given by

$$\mathbb{D} = \begin{bmatrix} \cos\theta & -\sin\theta \\ \sin\theta & \cos\theta \end{bmatrix} \begin{bmatrix} 1000 & 0 \\ 0 & 1 \end{bmatrix} \begin{bmatrix} \cos\theta & \sin\theta \\ -\sin\theta & \cos\theta \end{bmatrix}, \quad \theta = \pi/4,$$

where θ is the angle of the primary diffusion direction (parallel to the first eigenvector of $\mathbb{D}$).

This example satisfies the maximum principle and the solution stays between 0 and 2 and has sharp jumps near the inner boundary. The analytical solution is not available, but the numerical solution is provided in Fig. 6b. The goal is to produce a numerical solution which also satisfies DMP and stays between 0 and 2 and has a good adaptation.

In two dimensions and for the error measured in the H^1-semi-norm, the DMP-compliant anisotropic metric tensor $M_{DMP,K}$ developed in [29] is given element-wise by

$$M_{DMP,K} = \left(1 + \frac{1}{\alpha_h} B_{DMP,K}\right)^{\frac{1}{2}} \det\left(\mathbb{D}_K\right)^{\frac{1}{2}} \mathbb{D}_K^{-1}, \tag{9}$$

where

$$B_{DMP,K} = \det\left(\mathbb{D}_K\right)^{-\frac{1}{2}} \left\|\mathbb{D}_K^{-1}\right\| \cdot \frac{1}{|K|} \int_K \left\|\mathbb{D}_K \left|H(u)\right|\right\|^2 d\boldsymbol{x}. \tag{10}$$

The diffusion matrix $\mathbb{D}$ in (9) provides the correct mesh alignment whereas the Hessian of the exact solution in (10) is responsible for the appropriate mesh density. As noted in Sect. 2, if the finite element solution error can be bounded by the interpolation error of the hierarchical basis error estimator, the Hessian of the exact solution in (10) can be replaced by the Hessian of the HBEE z_h:

$$B_{HB,K} = \det\left(\mathbb{D}_K\right)^{-\frac{1}{2}} \left\|\mathbb{D}_K^{-1}\right\| \cdot \frac{1}{|K|} \int_K \left\|\mathbb{D}_K \left|H(z_h)\right|\right\|^2 d\boldsymbol{x}. \tag{11}$$

With this choice, the mesh will still satisfy the DMP, but this time the mesh density is determined by the *a posteriori* error estimate z_h.

To emphasize the compliance with the DMP, the metric tensors M_{DMP} and M_{DMP+HB} based on (10) and (11), respectively, are also compared to a uniform mesh and the anisotropic metric tensor M_{HB} based solely on the HBEE (Sect. 3). Figures 7 and 8 show meshes and solution contours.

No overshoots in the finite element solutions are observed for all cases, but Fig. 7 shows that undershoots and unphysical minima occur in the solutions obtained with the uniform mesh ($\min u_h \approx -0.059$) and M_{HB} ($\min u_h \approx -0.0032$). No undershoots can be observed for M_{DMP} and M_{DMP+HB} (Fig. 8). The results confirm the prediction that the solutions obtained with M_{DMP} and M_{DMP+HB} satisfy DMP and no unphysical extrema occur.

As for M_{DMP} and M_{DMP+HB}, the solution contours for both metric tensors are almost undistinguishable and, although not as smooth, still quite comparable to the one obtained with M_{HB} (cf. Figs. 8 and 7b), thus providing a good adaptation to the sharp solution jump near the interior boundary (cf. the somewhat smeared solution jump for the isotropic mesh in Fig.7a, right). The mesh computed by means of HBEE is fully comparable with the mesh obtained using Hessian recovery. Again, the maximum aspect ratio of the mesh obtained by means of the HBEE has a slightly larger aspect ratio.

6 Concluding remarks

Numerical results show that a global HBEE can be a successful alternative to Hessian recovery in mesh adaptation: in all three examples both methods provide very similar results. However, as observed in the heat conduction example in Sect. 3, Hessian recovery could result in unnecessarily high mesh density for problems with discontinuities. Also, it can cause a light mesh smoothing: meshes obtained by means of Hessian recovery-based method have a slightly smaller maximum aspect ratio than meshes obtained with HBEE and therefore seem to be slightly worse in terms of alignment with the steep boundary

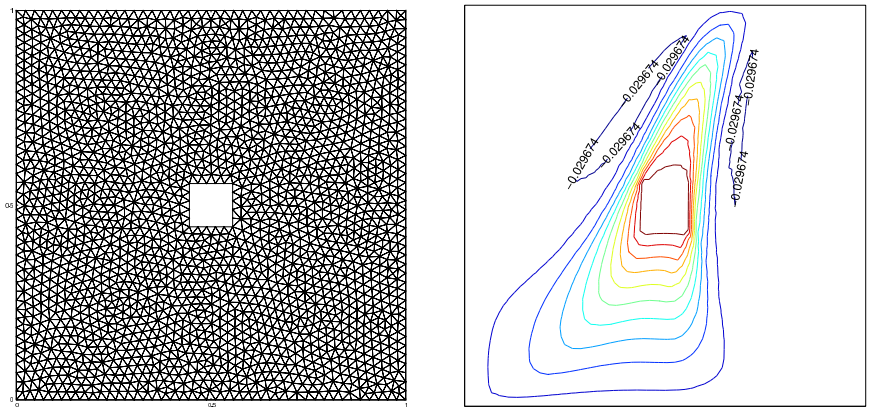

(a) Isotropic: 4170 triangles, $\min u_h \approx -5.9 \times 10^{-2}$, max. aspect ratio 2.7.

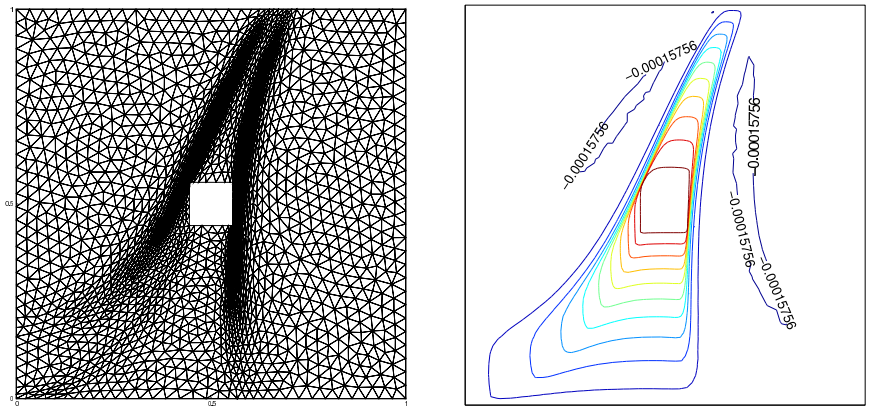

(b) M_{HB}: 4353 triangles, $\min u_h \approx -3.2 \times 10^{-4}$, max. aspect ratio 37.2.

Fig. 7: Anisotropic diffusion: meshes and contour plots of the numerical solution for the (a) isotropic and (b) HBEE-based M_{HB} metric tensors.

layers. The global HBEE seems to be less affected by these issues and, depending on the underlying problem, can provide a more robust solution.

A key component of the HBEE-based method is to find the solution z_h of the error problem (E_h). This is a global problem. Hence, finding its exact solution can be as costly as for computing a quadratic finite element approximation to the original problem. However, a fast approximate solution is as fast as Hessian recovery and proved to be sufficient to provide enough directional information for the purpose of the mesh adaptation.

Another key component of the method is the reliability of the error estimator on anisotropic meshes: error estimation with hierarchical bases is usually based on the saturation assumption, which basically states that quadratic approximations provide finer information on the solution than linear ones.

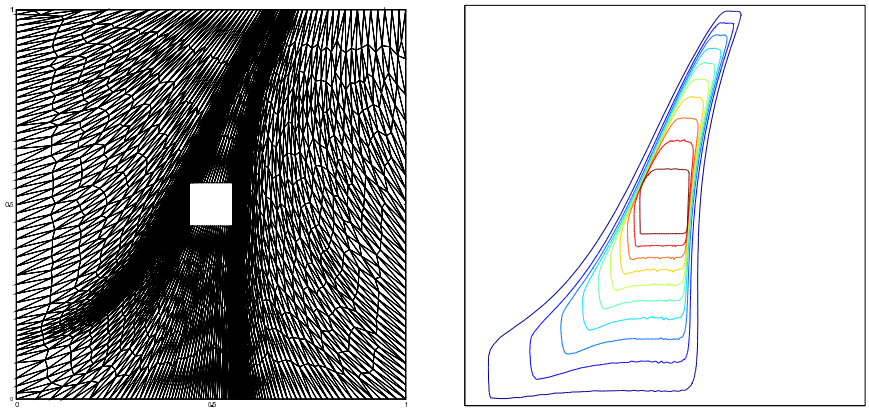

(a) M_{DMP}: 4253 triangles, no undershoots, max. aspect ratio 76.5.

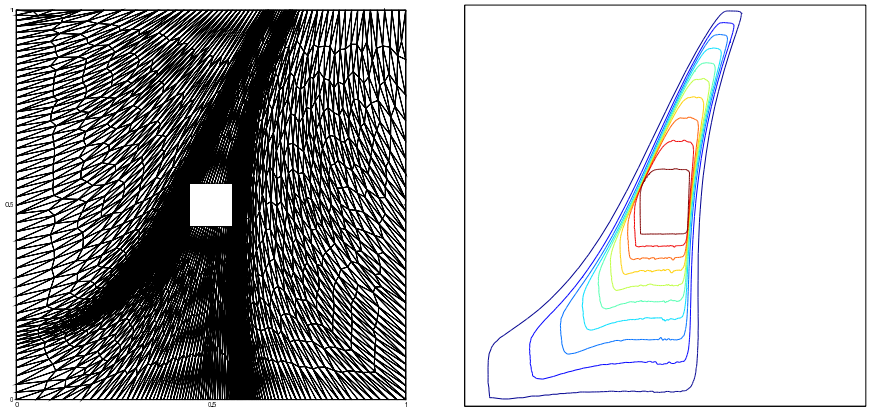

(b) M_{DMP+HB}: 4381 triangles, no undershoots, max. aspect ratio 84.2.

Fig. 8: Anisotropic diffusion: meshes and contour plots of the numerical solution for the (a) Hessian recovery-based M_{DMP} and (b) HBEE-based M_{DMP+HB} metric tensors.

Existing results on its validity require bounds on the elements' aspect ratio [18]. It is still unclear if similar results can be achieved for general adaptive meshes, but numerical results suggest that aspect ratio bounds are not necessary if the mesh is properly aligned. Moreover, it seems that good mesh adaptation does not require an accurate Hessian recovery or an accurate error estimator, but rather some additional information of global nature, although it is still unclear which information exactly is necessary.

Acknowledgements. This research was supported in part by the German Research Foundation (DFG) through the grant KA 3215/1-1. The author is grateful to the anonymous referees for their valuable comments.

References

1. Abdellatif Agouzal, Konstantin Lipnikov, and Yuri Vassilevski. Generation of quasi-optimal meshes based on a posteriori error estimates. In *Proceedings of the 16th International Meshing Roundtable*, pages 139–148, 2008.
2. Abdellatif Agouzal, Konstantin Lipnikov, and Yuri Vassilevski. Anisotropic mesh adaptation for solution of finite element problems using hierarchical edge-based error estimates. In *Proceedings of the 18th International Meshing Roundtable*, pages 595–610, 2009.
3. Abdellatif Agouzal, Konstantin Lipnikov, and Yuri Vassilevski. Hessian-free metric-based mesh adaptation via geometry of interpolation error. *Comput. Math. Math. Phys.*, 50(1):124–138, January 2010.
4. Abdellatif Agouzal and Yuri V. Vassilevski. Minimization of gradient errors of piecewise linear interpolation on simplicial meshes. *Comput. Methods Appl. Mech. Engrg.*, 199(33-36):2195–2203, 2010.
5. Thomas Apel, Sergei Grosman, Peter K. Jimack, and Arnd Meyer. A new methodology for anisotropic mesh refinement based upon error gradients. *Appl. Numer. Math.*, 50(3-4):329–341, 2004.
6. Randolph E. Bank and R. Kent Smith. A posteriori error estimates based on hierarchical bases. *SIAM J. Numer. Anal.*, 30(4):921–935, 1993.
7. Randolph E. Bank and Jinchao Xu. Asymptotically exact a posteriori error estimators, Part I: Grids with superconvergence. *SIAM J. Numer. Anal.*, 41(6):2294–2312, 2003.
8. Randolph E. Bank and Jinchao Xu. Asymptotically exact a posteriori error estimators, Part II: General unstructured grids. *SIAM J. Numer. Anal.*, 41(6):2313–2332, 2003.
9. Michael Bildhauer. *Convex variational problems. Linear, nearly linear and anisotropic growth conditions.*, volume 1818 of *Lecture Notes in Mathematics*. Springer Berlin / Heidelberg, X 2003.
10. Houman Borouchaki, Paul Louis George, Frédéric Hecht, Patrick Laug, and Eric Saltel. Delaunay mesh generation governed by metric specifications. Part I. Algorithms. *Finite Elements in Analysis and Design*, 25(1-2):61–83, 1997.
11. Houman Borouchaki, Paul Louis George, and Bijan Mohammadi. Delaunay mesh generation governed by metric specifications. Part II. Applications. *Finite Elem. Anal. Des.*, 25(1-2):85–109, 1997.
12. Weiming Cao, Weizhang Huang, and Robert D. Russell. Comparison of two-dimensional r-adaptive finite element methods using various error indicators. *Math. Comput. Simulation*, 56(2):127–143, 2001.
13. M. J. Castro-Díaz, F. Hecht, B. Mohammadi, and O. Pironneau. Anisotropic unstructured mesh adaption for flow simulations. *Int. J. Numer. Meth. Fluids*, 25(4):475–491, 1997.
14. P. G. Ciarlet and P. A. Raviart. Maximum principle and uniform convergence for the finite element method. *Comput. Methods Appl. Mech. Engrg.*, 2(1):17–31, 1973.
15. P. Deuflhard, P. Leinen, and H. Yserentant. Concepts of an adaptive hierarchical finite element code. *Impact Comput. Sci. Engrg.*, 1(1):3–35, 1989.
16. Manfred Dobrowolski, Steffen Gräf, and Christoph Pflaum. On a posteriori error estimators in the finite element method on anisotropic meshes. *Electron. Trans. Numer. Anal.*, 8:36–45, 1999.

17. Vít Dolejší. Anisotropic mesh adaptation for finite volume and finite element methods on triangular meshes. *Comput. Vis. Sci.*, 1(3):165–178, 1998.
18. Willy Dörfler and Ricardo H. Nochetto. Small data oscillation implies the saturation assumption. *Numer. Math.*, 91:1–12, 2002.
19. Luca Formaggia and Simona Perotto. New anisotropic a priori error estimates. *Numer. Math.*, 89(4):641–667, 2001.
20. Pascal Jean Frey and Paul-Louis George. *Mesh Generation. Second Edition*. John Wiley & Sons, Inc., Hoboken, NJ, 2008.
21. Frédéric Hecht. *BAMG: Bidimensional Anisotropic Mesh Generator*, 2006. Source code: `http://www.ann.jussieu.fr/~hecht/ftp/bamg/`.
22. Weizhang Huang. Measuring mesh qualities and application to variational mesh adaptation. *SIAM J. Sci. Comput.*, 26(5):1643–1666, 2005.
23. Weizhang Huang. Metric tensors for anisotropic mesh generation. *J. Comput. Phys.*, 204(2):633–665, 2005.
24. Weizhang Huang, Lennard Kamenski, and Jens Lang. A new anisotropic mesh adaptation method based upon hierarchical a posteriori error estimates. *J. Comput. Phys.*, 229(6):2179–2198, 2010.
25. Weizhang Huang, Lennard Kamenski, and Xianping Li. Anisotropic mesh adaptation for variational problems using error estimation based on hierarchical bases. *Canad. Appl. Math. Quart.*, to appear, arXiv:1006.0191, 2010.
26. Weizhang Huang and Xianping Li. An anisotropic mesh adaptation method for the finite element solution of variational problems. *Finite Elem. Anal. Des.*, 46(1-2):61–73, 2010.
27. Weizhang Huang and Wei Wei Sun. Variational mesh adaptation II: error estimates and monitor functions. *J. Comput. Phys.*, 184(2):619–648, 2003.
28. Lennard Kamenski. *Anisotropic Mesh Adaptation Based on Hessian Recovery and A Posteriori Error Estimates*. PhD thesis, TU Darmstadt, 2009.
29. Xianping Li and Weizhang Huang. An anisotropic mesh adaptation method for the finite element solution of heterogeneous anisotropic diffusion problems. *J. Comput. Phys.*, to appear, arXiv:1003.4530, 2010.
30. Jeffrey S. Ovall. The dangers to avoid when using gradient recovery methods for finite element error estimation and adaptivity. Technical Report 6, Max Planck Institute for Mathematics in the Sciences, 2006.
31. Jeffrey S. Ovall. Function, gradient, and Hessian recovery using quadratic edge-bump functions. *SIAM J. Numer. Anal.*, 45(3):1064–1080, 2007.
32. D. Pardo and L. Demkowicz. Integration of hp-adaptivity and a two-grid solver for elliptic problems. *Comput. Methods Appl. Mech. Engrg.*, 195(7-8):674–710, 2006.
33. Zhimin Zhang and Ahmed Naga. A new finite element gradient recovery method: Superconvergence property. *SIAM J. Sci. Comput.*, 26(4):1192–1213, 2005.
34. Olgierd Cecil Zienkiewicz and Jian Zhong Zhu. The superconvergent patch recovery and a posteriori error estimates. Part 1: The recovery technique. *Int. J. Numer. Methods Engrg.*, 33(7):1331–1364, 1992.
35. Olgierd Cecil Zienkiewicz and Jian Zhong Zhu. The superconvergent patch recovery and a posteriori error estimates. Part 2: Error estimates and adaptivity. *Int. J. Numer. Methods Engrg.*, 33(7):1365–1382, 1992.